Symmetry-Resolved Study of Lattice Vibration and Libration Modes in [Fe(phen)2(NCS)2] Crystal

Gaël Privault, Jean-Yves Mevellec, Maciej Lorenc, Bernard Humbert, Etienne Janod, Nathalie Daro, Guillaume Chastanet, Alaska Subedi, Eric Collet

Symmetry-resolved study of lattice vibration and libration modes in $[Fe(phen)_2(NCS)_2]$ crystal

Gaël Privault,[a] Jean-Yves Mevellec,[b,] Maciej Lorenc,[a,c] Bernard Humbert,[b] Etienne Janod,[b,c] Nathalie Daro,[d] Guillaume Chastanet,[d] Alaska Subedi[e,*] and Eric Collet [a,c]*

[a] Univ Rennes, CNRS, IPR (Institut de Physique de Rennes) - UMR 6251, F-35000 Rennes, France

[b] Nantes Université, CNRS, Institut des Matériaux Jean Rouxel, IMN, UMR 6502, F-44000 Nantes, France

[c] DYNACOM IRL2015 University of Tokyo - CNRS - UR1, Department of Chemistry, 7-3-1 Hongo, Tokyo 113-0033 - Japon

[d] Univ. Bordeaux, CNRS, Bordeaux-INP, ICMCB, UMR 5026, F-33600 Pessac, France

[e] CPHT, CNRS, Ecole Polytechnique, IP Paris, F-91128 Palaiseau, France

Abstract

In the family of spin crossover materials, which undergo thermal conversion between low-spin (LS) and high-spin (HS) phases, it is of great interest to study vibrational modes. On the one hand, vibration modes are characteristic of the spin state and vibrational spectroscopies are often used for monitoring spin-state switching driven by temperature, pressure or light. On the other hand, the spin-state thermal conversion is an entropy-driven process and the vibrational entropy change represents the main contribution to the total entropy difference between LS and HS phases at solid state. However, the discussion of vibrations in spin-crossover materials is often limited at the molecular scale. Here we study vibration modes in the $[Fe(phen)_2(NCS)_2]$ crystal, and we compare symmetry-resolved vibrational spectroscopy data performed on single crystal to DFT calculations performed in a periodic 3D crystal. We discuss the complex nature of vibrational modes in crystals, including vibration of molecules within the crystalline lattice, with different symmetries and frequencies. We also highlight the presence of many low frequency libration modes of different symmetries. The contribution of vibrational entropy, added to the electronic entropy, provides a total entropy difference in the solid state, which is in very good agreement with calorimetric measurements.

Introduction

In spin-transition or spin-crossover materials, a good knowledge of vibration modes is of great importance for characterizing changes of molecular states, as vibrational spectra are characteristic of the spin state due to coupled electronic – structural reorganizations.[1-6] In this way, vibrational spectroscopy is often used to characterize spin-state switching induced by temperature, pressure or light.[7-8] The splitting of vibrational modes can also provide a nice signature of symmetry breaking.[9-12] Vibration modes play a key role for understanding entropy-driven phase transitions at thermal equilibrium due to their important contribution to vibrational entropy.[7, 13-21] In addition, during photoinduced out-of-equilibrium spin-state switching, the coupled structural dynamics involves coherent molecular vibrations, allowing for ultrafast spin-state switching.[22-27] There are numerous experimental and theoretical studies of vibrational modes in molecular spin-crossover materials. However, the description of vibrations in molecular crystals is often limited to the description of intra-molecular modes of isolated molecules, which is too limiting because vibration modes of molecules in crystals are not simple superpositions of intra-molecular modes. On the one hand, molecules in crystals exhibit libration modes, corresponding to a mixing of molecular displacements and rotation. On the other hand, the crystal design and its symmetry include several molecules within the unit cell and generates different molecular vibrations with the same nature but different symmetries and frequencies.

Here we study the prototype $[Fe(phen)_2(NCS)_2]$ spin crossover system (SCO).[13, 27-31] At atmospheric pressure it undergoes a weakly first-order phase transition around 176 K on warming, from LS (S=0, $t_{2g}^6 e_g^0$) to HS (S=2, $t_{2g}^4 e_g^2$) states, where t_{2g} and e_g orbitals refer to Fe d-orbitals. In this work we combine symmetry-resolved vibrational spectroscopies (Raman and infrared) and lattice mode calculations based on the frozen mode method. We show that polarized spectroscopic

measurements allow for disentangling the different modes with different symmetries, including low frequency libration modes or molecular breathing modes. In this way, we estimate the contribution of the vibrational entropy change in the frame of crystalline vibrations instead of molecular vibrations, considering the global change of vibrational entropy between LS and HS states. The results show that many low frequency modes are a mixture of libration and intra-molecular modes. The obtained entropy difference between HS and LS state, including electronic entropy and vibrational entropy, is in very good agreement with heat capacity measurement.[17]

Experimental Section

Single crystals of $[Fe(phen)_2(NCS)_2]$ compound were obtained by slow diffusion adapted from Gallois *et al.* protocol.[32] The $FeSO_4.7H_2O$, KNCS and 1,10-phenanthroline (phen) reactants were used as purchased. The methanol is purified by distillation over Mg under inert atmosphere prior to use. A solution at 1.10^{-3} mol of $Fe(NCS)_2$ in 10 mL of methanol (from the reaction of $Fe(SO_4)_2.7H_2O$ and KNCS) and a solution at 2.10^{-3} mol of 1,10-phenanthroline in 10 mL of methanol were firstly prepared. The single crystals were obtained after few days by slow diffusion of the two solutions in a H-shape tube under inert atmosphere (1 or 2 mL of the two reactants separated with methanol). The single crystals form lozenge plates and we checked crystalline orientations by X-ray diffraction. The short lozenge diagonal is the crystalline axis ***a***, the long one is the ***b*** axis and the perpendicular direction corresponds to the ***c*** axis.[26-27, 33]

We performed symmetry-resolved vibrational spectroscopy analysis on $[Fe(phen)_2(NCS)_2]$ single crystals. Infrared specular reflectance data (at angle 0°) were obtained on a Hyperion 2000 microscope coupled with a Bruker vertex 70 spectrometer. The analyzed surface was 100 µm

diameter focused with a Cassegrain objective (x20). The collecting cone for this objective had an effective half angle of 23.6° (numerical aperture 0.4), as in the case of Raman microscopy (30°), the polarization leaks are still limited at these angles. For these both techniques, the spectral resolution was smaller than 4 cm^{-1} FWHM. As previously, we used the HFS600E-PB4 stage from Linkam to perform IR reflectance measurements in the LS phase (95 K) by replacing the quartz window with a ZnSe window. By inserting a KRS-5 polarizer, we collected the reflected IR polarized light for probing the vibration modes with symmetries B_{2u} (*y* polarization), B_{1u} (*z*) or B_{3u} (*x*). Additional data are shown in Figure S1.

Raman Spectroscopy measurements were recorded with an Invia Spectrometer from Renishaw, with two different laser wavelengths: 633 nm obtained from a He-Ne laser and 785 nm with a laser diode. The microscope objective (x50) focused the laser on a ≃4 μm^2 spot on a single crystal, the laser power was limited at 0.1 mW to avoid local heating. The low wavenumbers (until 20 cm^{-1}), like antiStokes bands, were observed using eclipse filters (Bragg gratings) rather than a notch filter. We studied the HS state at room temperature and we used a HFS600E-PB4 stage from Linkam to study the LS phase at low temperature phase (130 K). Incident excitation light was linearly polarized along the ***a*** (*x*), ***b*** (*y*) or ***c*** (*z*) crystalline axes.[28] In the backscattering configuration of the microscope, we probed both parallel and perpendicular polarizations of backscattered Raman signals by using a linear analyzer for the output. Moreover, a half-wave plate is then added so that the light falls in the same way on the grating. In this way, we could selectively probe the modes with Symmetries A_g (*xx*, *yy* or *zz* polarizations), B_{1g} (*xy*), B_{2g} (*xz*) or B_{3g} (*xy*). Additional data are shown in Figures S2 and S3.

Theoretical Calculations

The phonon calculations at the Brillouin zone center were performed using the frozen-phonon method as implemented in the PHONOPY package.[34] This required generating 153 structures with different atomic displacements in the 204-atom unit cell of this material. Atomic forces due to the displacements were calculated from first principles using the QUANTUM ESPRESSO package.[35] This is a pseudopotential-based planewave code, and we used the pseudopotentials generated by Garrity et al.[36] The exchange and correlation interactions were treated using the optB88-vdW functional that accurately treats the van der Waals interactoin.[37] Basis-set and charge-density expansion were done using 50 and 300 Ry, respectively. A 3×4×2 grid was used in the Brillouin zone integration. These calculations were performed using fully relaxed structures. The lattice parameters obtained for the low-spin phase are $\boldsymbol{a}$ = 12.7895 Å, $\boldsymbol{b}$ = 9.8959 Å and $\boldsymbol{c}$ = 16.8703 Å and for the high-spin phase are $\boldsymbol{a}$ = 13.2098 Å, $\boldsymbol{b}$ = 9.8628 Å, and $\boldsymbol{c}$ = 16.9282 Å are in good agreement with experimental data. [26-27] The DFT calculations provide then for each mode three important characteristics: the frequency, the symmetry of the modes, as well as the atomic motions involved. Since the unit cell contains four molecular units made of 51 atoms, there are 51×4×3=612 phonon modes at the center of the Brillouin zone (3 acoustic and 609 optic). Since the 4 Fe atoms lie on the $C_2(y)$ Wyckoff position and the 200 other atoms are in general position, the 612 atomic vibration modes in the crystal at the Γ point of the Brillouin zone decompose according to:

$\Gamma_T = 76A_g+76A_u+76B_{2g}+76B_{2u}+77B_{1g}+77B_{3g}+77B_{1u}+77B_{3u}$.

Table S2 includes the frequencies of the A_g, A_u, B_{2g}, B_{2u}, B_{1g}, B_{1u}, B_{3g} and B_{3u} modes calculated with the frozen mode method and numbered with increasing frequency.

Results and Discussion

The $[Fe(phen)_2(NCS)_2]$ materials crystalizes in the Pbcn space group (Figure 1), with a general multiplicity of 8.[30, 33] The asymmetric unit corresponds to $Fe_{0.5}$(phen)(NCS), as the Fe atom is lying on a Wyckoff position of C_2 symmetry and the other $Fe_{0.5}$(phen)(NCS) unit is equivalent by $C_2(y)$ axis along the crystalline axis ***b***. There are 6 additional $Fe_{0.5}$(phen)(NCS) units in the unit cell, equivalent by the different symmetry operators of the space group: the screw axes 2_1(//***a***) and 2_1(//***c***), the glide planes b ($\perp$ ***a***), c ($\perp$ ***b***) and n ($\perp$ ***c***) as well as inversion symmetry in between molecules. As shown in Figure 1, there are 4 molecules in the unit cell at Wyckoff positions (0,y,¼), (½ ,–y+½,¾), (0,–y,¾) and (½,y+½,¼). Therefore the 612 vibrations of molecules in the crystal generated by these symmetry operators are much complex than the 147 intra-molecular vibrations of isolated molecules. For describing the symmetry of the modes at the Γ point of the Brillouin zone, we use the *mmm* point group (D_{2h}, Table S1), corresponding to the Pbcn space group. The 2_1 axes correspond to $C_2(x)$ and $C_2(z)$ axis, while the glide planes b, c and n correspond respectively to $\sigma(yz)$, $\sigma(xz)$ and $\sigma(xy)$.

For pedagogical purpose, we discuss the complexity of vibrational modes with the example of the N↔CS stretching modes. For the isolated molecule, [13, 15, 33, 38-39] there are 2 N↔CS stretching modes: one symmetric with respect to $C_2(y)$ molecular axis with in-phase elongations of the two N↔CS, and one antisymmetric with out-of-phase elongations. At crystalline state, since there are 8 equivalent NCS groups in the unit cell, there are 8 N↔CS stretching modes; one for each of the 8 representations of the point group, as shown in Figure 2 and listed in Table S1. A_g, A_u, B_{2g}, B_{2u} modes are symmetric with respect to the $C_2(y)$ molecular axis, while B_{1g}, B_{3g}, B_{1u}, B_{3u} modes are antisymmetric (supplementary video 1).

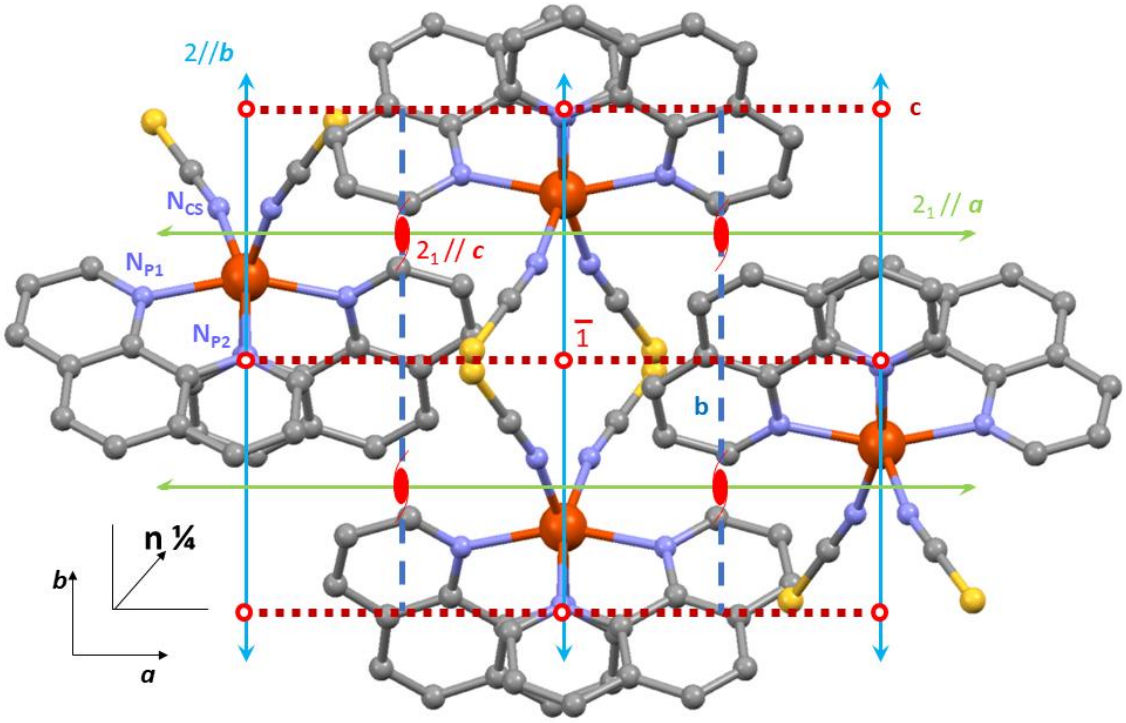

Figure 1. Molecular packing of within $[Fe(phen)_2(NCS)_2]$ crystal, showing 8 half molecules equivalent by the symmetry operators of the Pbcn space group: the 2-fold axis along ***b***, the 2_1 screw axes along ***a*** and ***c***, the glide planes b, c and n and the inversion symmetry ($\bar{1}$).

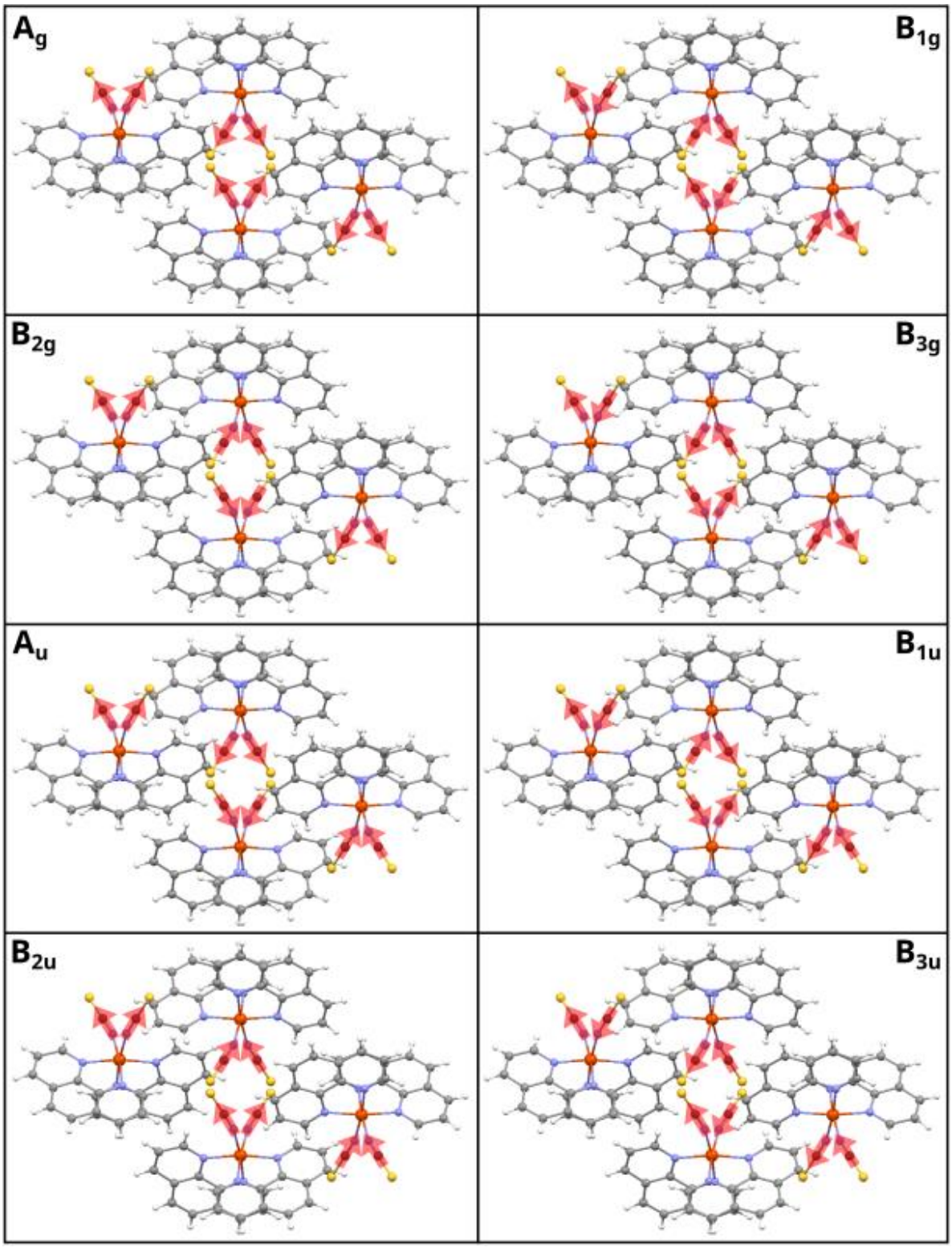

Figure 2. Schematic representation of the 8 N↔CS stretching modes with different symmetries. The red arrows represent the relative motion of the N and C atoms (see supplementary video 1).

Figure 3 shows symmetry-resolved vibrational spectra obtained from a single crystal of $[Fe(phen)_2(NCS)_2]$. As indicated in Table S1, Raman-active modes of symmetry A_g, B_{3g}, B_{2g} and B_{1g}, can be selectively probed by Raman spectroscopy by adjusting the polarization of the incoming laser beam and/or the polarization of backscattered Raman signals with respect to crystalline axes. A_g modes were probed with an incident light polarization and backscattered Raman both parallel to crystalline axis ***b*** (*yy* configuration), while B_{3g}, B_{2g} and B_{1g} spectra were probed in *xy*, *xz* and *yz* configurations. The B_{3u}, B_{2u} and B_{1u} IR-active modes were selectively probed by FT-IR reflectivity with polarization along crystalline directions *x*, *y*, or *z* respectively. The A_u modes are not Raman nor IR active. Spectra are shown for the HS state measured at room temperature, with some LS spectra measured at 130 K as well. The 4 Raman and 3 IR active N↔CS stretching modes shift from ≃ 2070 cm^{-1} in the HS state to ≃ 2110 cm^{-1} in the LS state. Figure S1 shows the absorption of the B_{1u}, B_{2u} and B_{3u} IR active N↔CS modes, obtained by Kramers-Krönig transformation of the polarized IR reflectivity spectra on single crystal. The IR absorption spectrum measured on a powder sample corresponds well to the superposition of the absorption of the 3 modes around 2061, 2064 and 2076 cm^{-1}, which result apparently in two bands due to overlapping.

We list in Table 1 the measured and calculated frequencies of the 8 N↔CS stretching modes of different symmetries shown in Figure 2. Figure 4 shows the evolution of the vibrational spectra computed for the LS and HS phases for the modes with different symmetries. Since the 8 N↔CS modes are the only ones in the 1700 – 3100 cm^{-1} frequency range (Table S2 and Figure 4), the identification of the nature of the modes is easy with atomic motions limited to N and C atoms of the NCS groups (supplementary video 1). In the LS state, the calculated frequencies are found around 2108 cm^{-1} for A_g, A_u, B_{2g} and B_{2u} modes symmetric with respect to the $C_2(y)$ axis, and

around 2099 cm^{-1} for B_{1g}, B_{3g}, B_{1u} and B_{3u} modes. In the HS state these values decrease to 2048 cm^{-1} and 2034 cm^{-1}. DFT calculation on isolated $[Fe(phen)_2(NCS)_2]$ molecule [13, 15, 38-39] also indicated that the mode symmetric with respect to the C_2 molecular axis is at slightly higher frequency than the antisymmetric mode. Our DFT calculations are in quite good agreement with experimental data and the frequency shift between HS and LS states is calculated at $\Delta\nu = 62$ cm^{-1}, compared to 44 cm^{-1} for experimental data.

Table 1. Measured and calculated frequencies of the 8 N↔CS stretching modes of different symmetries.

N↔CS modes	ν_{LS} (cm^{-1})	ν_{HS} (cm^{-1})	$\Delta\nu$ (cm^{-1})
A_g measured	2113	2069	44
A_g calculated	2108	2048	60
B_{2g} measured		2067	
B_{2g} calculated	219	2048	61
A_u measured			
A_u calculated	2106	2045	61
B_{2u} measured	2108	2061	47
B_{2u} calculated	2107	2051	57
B_{1g} measured	2106	2062	44
B_{1g} calculated	2100	2034	66
B_{3g} measured		2067	
B_{3g} calculated	2101	2038	62
B_{1u} measured		2064	
B_{1u} calculated	2097	2032	65
B_{3u} measured	2117	2076	41
B_{3u} calculated	2097	2031	65

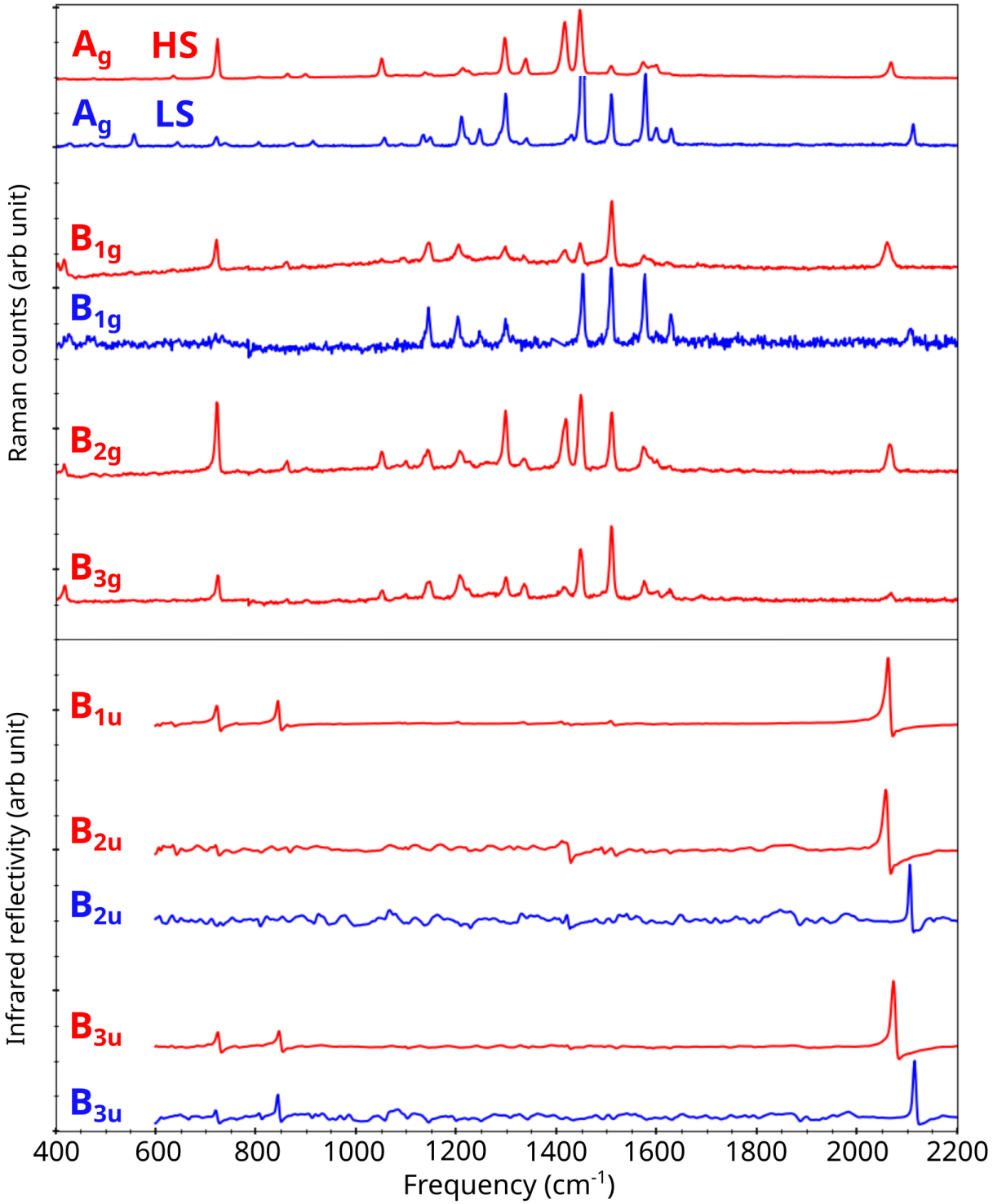

Figure 3. Symmetry-resolved high frequency Raman (top) and IR (bottom) spectra, with high spin (HS) state in red and low spin (LS) state in bleu.

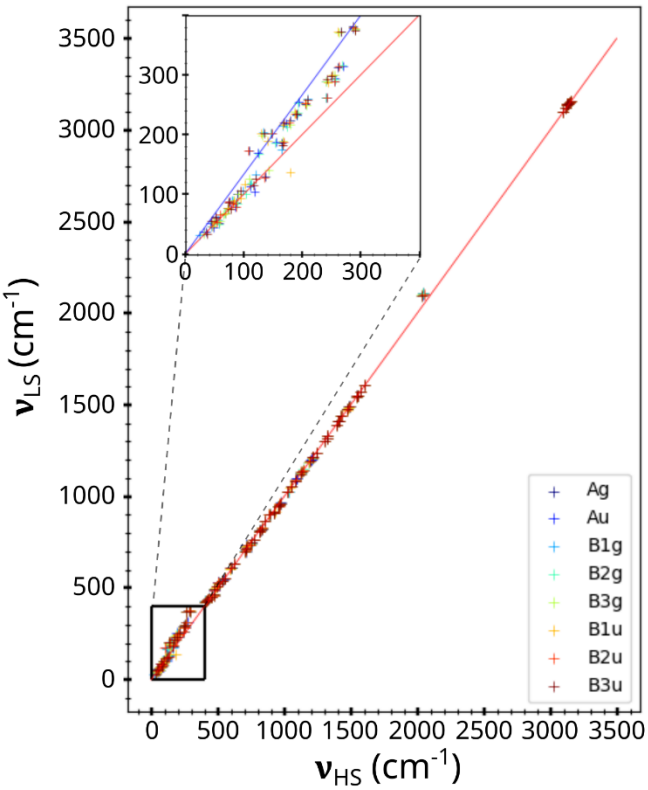

Figure 4. Evolution of vibrational frequencies of modes with different symmetries, computed for the HS and LS crystalline lattices of $Fe(phen)_2(NCS)_2$. The red line corresponds to $\frac{\nu^{LS}}{\nu^{HS}}$=1 and the blue one (inset) corresponds to $\frac{\nu^{LS}}{\nu^{HS}}$=1.33.

Figure 4 highlights important frequency shifts below 400 cm^{-1}. The discussion above about the splitting of the 8 N↔CS stretching modes of different symmetries is also relevant for many other modes, for which vibration is localized. For example, there are also 8 NC↔S stretching modes corresponding to A_g, B_{2g}, B_{2u}, B_{1g}, B_{3g}, B_{1u} and B_{3u} symmetries. In our calculation, these NC↔S modes are found around 820 cm^{-1}, while for isolated molecules the frequencies are found around 770 cm^{-1} or 850 cm^{-1}.[13, 38] Our experimental and theoretical data reveal different modes in this frequency range, including Fe-N and ligand stretching modes. We assign the NC↔S modes to the modes with different symmetries observed around 850 cm^{-1}.

It is well-known that the frequencies of the Fe-N stretching modes of the FeN_6 octahedron are strongly affected by the change of spin state, because in the LS state (S=0, $t_{2g}^6 e_g^0$) the Fe-N bonds are stronger than in the HS state (S=2, $t_{2g}^4 e_g^2$). For $Fe(phen)_2(NCS)_2$, a totally symmetric breathing mode was identified as shifting from 151 (LS) to 97 cm^{-1} (HS).[8, 13, 27-29] For a perfect FeN_6 octahedron with O_h point symmetry, there is a single totally symmetric A_g breathing mode, for which the 6 Fe-N bonds elongate in phase.[22] However, describing the totally symmetric nature of breathing modes is more difficult in the case of $Fe(phen)_2(NCS)_2$. On the one hand, the molecule is made of 3 independent N atoms (N_{CS}, N_{P1} and N_{P2} as shown in Figure 1), which result in 3 totally symmetric Fe-N breathing modes of A symmetry in the C_2 molecular point group. On the other hand, Fe-N stretching modes also couple to ligand modes (torsion and stretching). Consequently, there are many intra-molecular modes exhibiting Fe-N stretching character. There are 3 types of Fe-N stretching modes: the breathing modes with in-phase elongations of the 6 Fe–N bonds on a given molecule, the stretching modes symmetric with respect to the *C2(y)* molecular axis and the antisymmetric stretching ones. In our DFT calculations, the A_g mode exhibiting frequency shift from 109 cm^{-1} (HS) to 174 (LS), has a pronounced breathing nature of the phenanthroline ligand and especially Fe-N_{P1} bonds, while the Fe-NCS bonds are mainly bending. The A_u mode shifting from 124 cm^{-1} (HS) to 170 (LS), the B_{2g} mode shifting from 127 cm^{-1} (HS) to 167 (LS) and the B_{2u} mode shifting from 107 cm^{-1} (HS) to 172 (LS) exhibit similar in-phase breathing of 2 molecules and out-of-phase breathing of 2 others molecules in the unit cell (supplementary video 2). Figures S2 and S3 show additional Raman measurements performed with *xx*, *yy* and *xy* configurations and 785 nm probe. In average, the frequencies of these different breathing modes increase by ≃50% between HS and LS states. Figure 5 shows low frequency modes observed here with Raman spectroscopy and TD-THz spectroscopy data for the B_{2u} and B_{3u}

modes published previously.[28] The A_g Raman data confirm the frequency increase by more than 50% of the breathing mode from LS (161 cm^{-1}) to HS (101 cm^{-1}) states. These data also show several modes with different symmetries but similar frequencies, which can be identified as breathing modes of different symmetries in the HS state: A_g (101 cm^{-1}), B_{2g} (97 cm^{-1}) and B_{2u} (93 cm^{-1}). Similar conclusions are found from calculations for others symmetric stretching modes. The A_g mode shifting from 165 (HS) to 186 cm^{-1} (LS) exhibits in-phase stretching of the Fe-N_{P1} bonds, while the Fe-N_{P2} bonds stretch out-of-phase and the Fe-NCS parts are mainly bending. There are 3 corresponding modes with same character with symmetries B_{2g} (shifting from 153 to 185 cm^{-1}), B_{2u} (168 to 188 cm^{-1}) and A_u (156 to 187 cm^{-1}). The A_g mode shifting at 145 cm^{-1} (HS) exhibits in-phase stretching of the Fe-N_{P2} bonds and there are 3 corresponding modes with same character with symmetries B_{2g} (147 cm^{-1}), B_{2u} (147 cm^{-1}) and A_u (149 cm^{-1}). The Raman data for the A_g modes in Figure 5 confirm large frequency increase for other modes from 128, 166, 175 and 281 cm^{-1} in the HS state to 176, 196, 247 and 373 cm^{-1} in the LS state, which corresponds roughly to $\frac{\nu^{LS}}{\nu^{HS}} = 1.33$ (inset Figure 4). In this frequency range, our calculations reveal also antisymmetric Fe–N stretching modes with B_{1g}, B_{1u}, B_{3g}, B_{3u} symmetries and almost rigid ligand. There are higher frequency modes exhibiting both Fe–N and ligand stretching character, such as HS A_g modes at 718, 1052, 1212, 1308, 1328, 1429 or 1542 cm^{-1}. However, these modes at high frequency are not so populated, even at room temperature, and their contribution to vibrational entropy is limited. Therefore, we focus our attention on low frequency modes below 400 cm^{-1}.

In addition to vibrational modes localized around the FeN_6 octahedron, there are low frequency modes localized on the ligand, such as the butterfly modes of the phen. The 8 symmetry-equivalent phenanthroline groups in the unit cell give rise to 8 butterfly modes, corresponding to the different

symmetries in the crystal. There are 4 symmetric butterfly modes with respect to $C_2(y)$ molecular axis; A_g (HS: 137 cm^{-1}, LS: 129 cm^{-1}), A_u (HS: 117 cm^{-1}, LS: 104 cm^{-1}), B_{2g} (HS: 103 cm^{-1}, LS: 100 cm^{-1}), B_{2u} (HS: 135 cm^{-1}, LS: 128 cm^{-1}) and 4 asymmetric butterfly; B_{1g} (HS: 120 cm^{-1}, LS: 90 cm^{-1}), B_{1u} (HS: 140 cm^{-1}, LS: 137 cm^{-1}), B_{3g} (HS: 142 cm^{-1}, LS: 142 cm^{-1}), B_{3u} (HS: 119 cm^{-1}, LS: 126 cm^{-1}). The frequency of the modes strongly depends on symmetry, which dictates the relative motion of one ligand with respect to the ones of adjacent molecules.

The frequency splitting of the modes with symmetries is characteristic of their partial libration nature. Indeed, for molecular crystals in addition to intra-molecular modes, there are inter-molecular modes. On the one hand, inter-molecular modes in crystals combine intra-molecular vibrations to generate lattice modes of different symmetries, as explained above for the 8 N↔CS modes for example. On the other hand, there are many low frequency libration modes, mixing in a first approximation molecular rotations and translation, which can also contribute to vibrational entropy and which are often neglected with molecular-based approaches of vibrational spectra.[3]

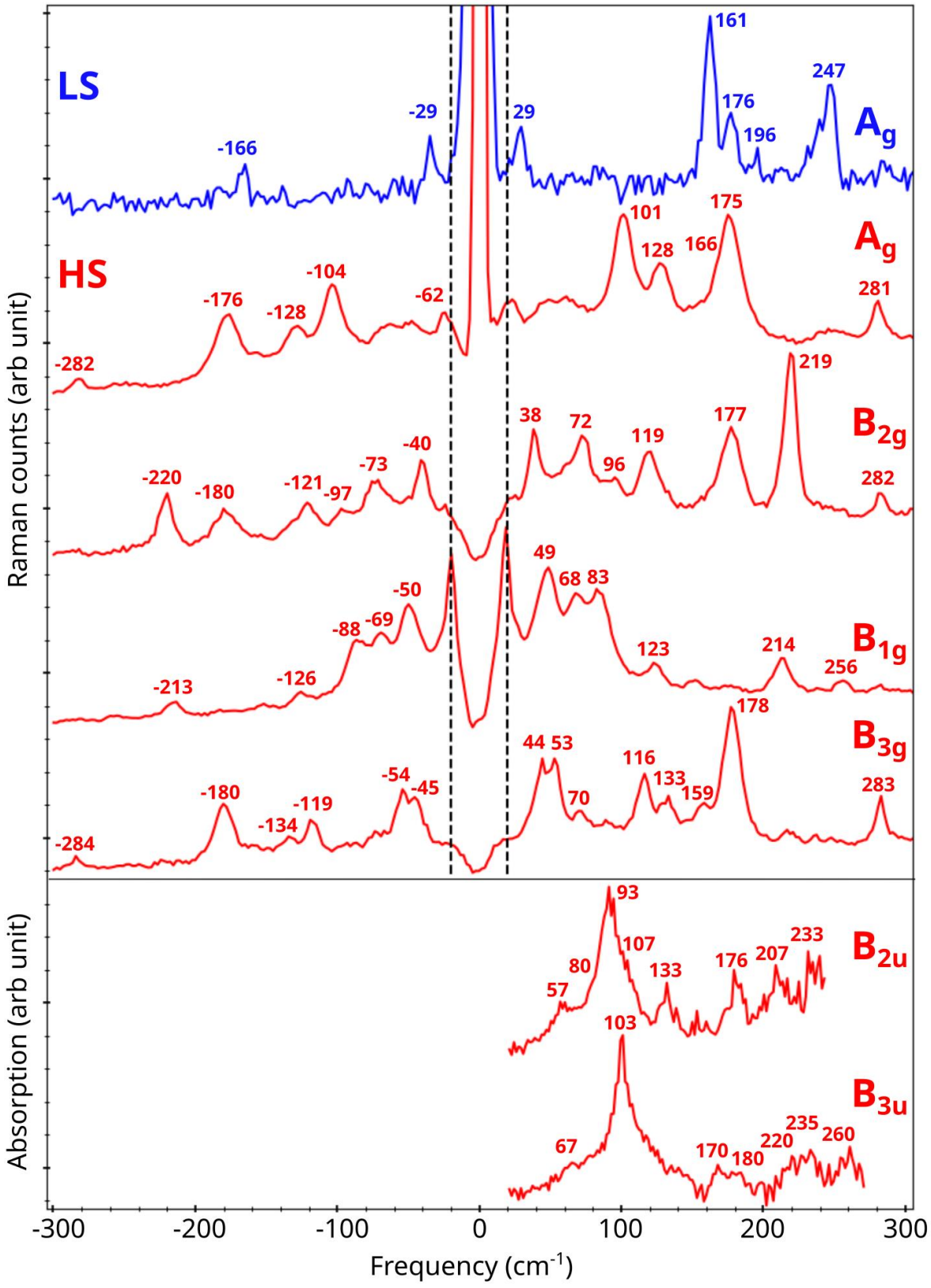

Figure 5. Low frequency and symmetry-resolved Raman (top) and IR (bottom) spectra.

Libration modes can be introduced in the frame of the rigid body approximation: each "half molecule" is considered as rigid with 6 degrees of freedom (3 translations + 3 rotations). In the case of $[Fe(phen)_2(NCS)_2]$ there are therefore 24 libration modes, including 3 acoustic modes. Because libration modes involve heavy particles and weak bonding compared to intra-molecular covalent bonds, their frequencies often fall below 100 cm^{-1}. Figure 5 shows that there are many modes, of different symmetries, in this spectral range. Most of DFT calculations performed on spin transition materials focused on isolated molecules and discussions of libration modes are lacking in the literature. Periodic DFT calculations were also performed on the same compound, but the analysis focused on the role of localized ligand–iron vibrations (110 – 430 cm^{-1}) and projected out translational and rotational motions of molecules in the crystal.[40] We will show hereafter that some libration modes can exhibit a significant contribution to vibrational entropy change due to their low frequency and large relative shift between HS and LS states.

High frequency modes like the 8 N↔CS modes have strongly localized intramolecular nature, as other atoms are almost frozen moving. However, in the low frequency range many modes have both intra-molecular and libration nature, with a relative translation of the center of mass of the molecules within the crystal or rotation of the molecular axes. Most of the modes strongly affected by the spin transition (Figure 4) have more or less pronounced libration nature. This means that in addition to the intra-molecular reorganization accompanying spin transition, the anisotropic lattice contraction can strongly affect the libration modes as the lattice parameters ***a*** and ***c*** increase on warming, while ***b*** decreases.[30] The libration nature of the "intramolecular" modes within the crystal translates in the splitting of their frequencies, and their different changes upon spin transition, due to inter-molecular (re)organization. This is the case for example of the breathing modes, with ≃20% frequency splitting of A_g, A_u, B_{2g} and B_{2u} modes (107–127 cm^{-1} for HS and 167–174 cm^{-1}

for LS) or ≃30% frequency splitting of butterfly modes (103–137 cm^{-1} range for HS and 100–129 cm^{-1} for LS). These frequencies are higher in our solid-state calculation compared to calculations on isolated molecules,[13, 38] which may be also due to the partial libration nature of the modes. On the contrary, the localized N↔CS stretching modes exhibit almost no libration nature with a very limited frequency splitting <0.2% for symmetric (A_g, A_u, B_{2g} and B_{2u} 2106-2009 cm^{-1}) or antisymmetric (B_{1g}, B_{3g}, B_{1u} and B_{3u} 2097-2101 cm^{-1}) modes.

There are also lattice modes with pronounced libration nature and limited intra-molecular motions. Figure 6 and video 3 show different types of libration modes. Mode number 4 (HS) with B_{1g} symmetry corresponds to a relative sliding of almost rigid molecular layers and its frequency increases by 30 % from HS (24.2 cm^{-1}) to LS (31.5 cm^{-1}). Mode number 5 (HS) with B_{3g} symmetry corresponds to rigid molecular rotation / translation and its frequency increases from 32 (HS) to 34.4 cm^{-1} (LS). Mode number 7 (HS) with A_g symmetry is a screwing mode corresponding to a rotation around the $C_2(y)$ axis and a translation along *y*. Its frequency is weakly affected by spin-state change (from 36.1 cm^{-1} to 36.3 cm^{-1}). Mode number 14 (HS) with symmetry B_{2g} also exhibits combined rotation and translation and its frequency increases from 49 to 53.1 cm^{-1}. Mode number 16 (HS) with B_{3g} symmetry corresponds to a dimerization mode of molecular layers and its frequency increases from 50.2 to 50.8 cm^{-1}.

These results illustrate that vibrational modes in molecular crystals have various natures, such as molecular translation or rotation, molecular breathing or torsion, as well as bond stretching or bending. In many cases the modes have hybrid characters. However, many low frequency modes exhibit large frequency shifts during spin state switching, with $1 < \frac{\nu^{LS}}{\nu^{HS}} < 1.33$ (Figure 4), and contribute therefore strongly to vibrational entropy.

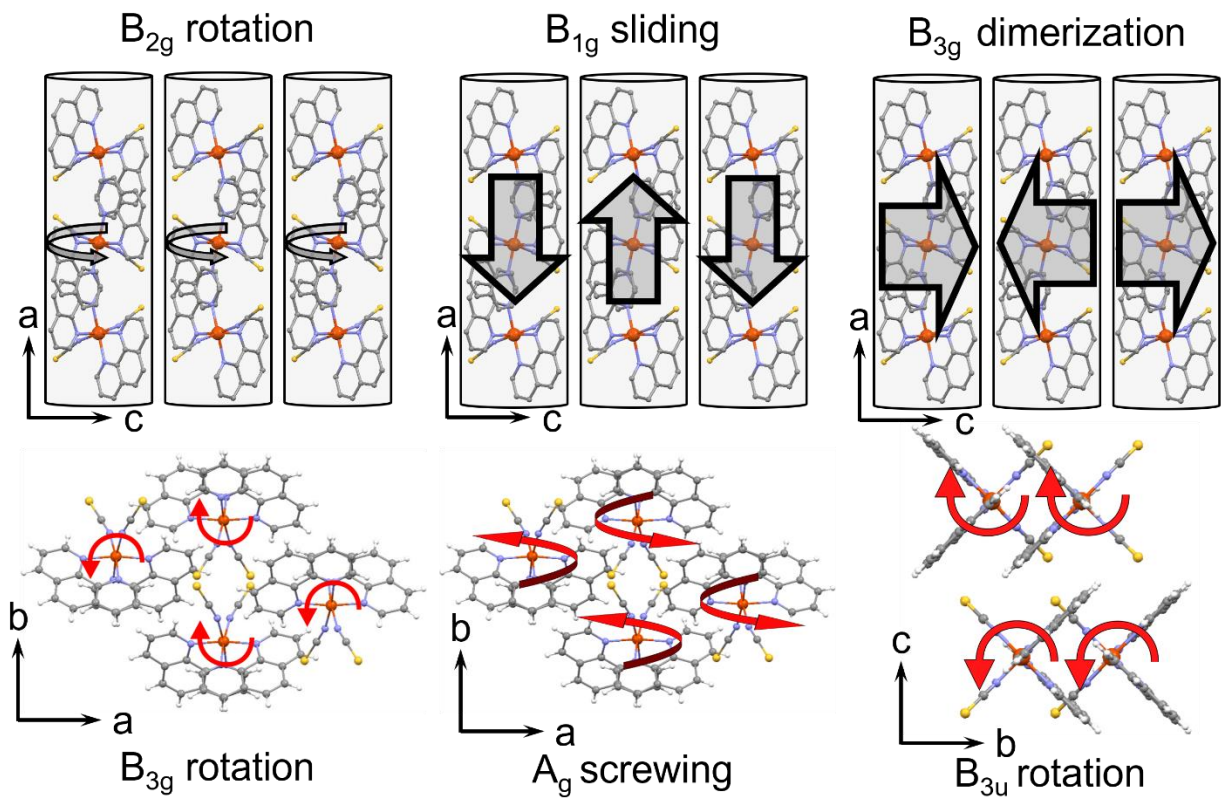

Figure 6. Libration modes of $[Fe(phen)_2(NCS)_2]$ molecules within the crystalline network, for which almost rigid molecule exhibit relative translations and/or rotations.

As recently reviewed by Nicolazzi,[3] the spin crossover phenomena at thermal equilibrium can be understood through the Gibbs energy difference between the HS and LS phases:

$$\Delta G = \Delta H + T\Delta S \qquad (1)$$

where ΔH represents the enthalpy difference between HS and LS states[3, 41] and $\Delta S = S^{HS} - S^{LS}$ is the entropy difference.[3, 7, 13-21]. For $[Fe(phen)_2(NCS)_2]$ $\Delta S = 48.78$ J.K^{-1}.mol^{-1} was extracted from calorimetric measurements.[17, 42] ΔS includes different contributions, due to the different microstates accessible in HS and LS configurations:

$$\Delta S = \Delta S_{el} + \Delta S_{vib} + \Delta S_{trans} + \Delta S_{rot} \qquad (2)$$

ΔS_{el} is the electronic entropy variation, which originates from the different numbers of microstates, characterized by different spin (and eventually orbital) momenta, accessible in HS and LS states. For an Fe^{II} system like $[Fe(phen)_2(NCS)_2]$ the spin multiplicity changes from 5 in HS (S=2) state to 1 in the (S=0) state. Therefore, the electronic contribution to entropy change, $\Delta S_{el} = Rln(5) = 13.38$ J.K^{-1}.mol^{-1}, represents only a small fraction of the entropy change.

The vibrational entropy difference $\Delta S_{vib} = S_{vib}^{HS} - S_{vib}^{LS}$ is associated with the frequency changes from ν_λ^{LS} to ν_λ^{HS} of different vibration modes λ between LS and HS states, which modify phonon populations and therefore HS and LS vibrational entropies. In the low frequency approximation, where $h\nu_\lambda \ll kT$, the vibrational entropy can be simplified[8] and reaches

$$\Delta S_{vib} = R \sum_\lambda \ln\left(\frac{\nu_\lambda^{LS}}{\nu_\lambda^{HS}}\right) \qquad (3)$$

There are many modes for which $1 < \frac{\nu^{LS}}{\nu^{HS}} < 1.33$ (inset Figure 4) and therefore $\Delta S_{vib} > 0$.

Different approaches were proposed in the literature to estimate ΔS_{vib} for $[Fe(phen)_2(NCS)_2]$, based on IR and Raman measurements and DFT calculations.[6, 8, 13, 15] By considering mainly the

15 vibration modes of an idealized Fe-N_6 octahedron, the vibrational entropy difference was estimated to 20 J.K^{-1}.mol^{-1}, with a significant contribution of the breathing mode to ΔS_{vib} = 2–4 J.K^{-1}.mol^{-1} due to its huge frequency shifts. By using the approximation that the 15 vibrations modes λ of the FeN_6 octahedron are equally affected by the change of spin state, with $\frac{\nu_\lambda^{LS}}{\nu_\lambda^{HS}}$ = 1.3, the vibrational entropy difference was estimated to 32.7 J.K^{-1}.mol^{-1}. By assessing individual contributions from different vibrational modes, Ronayne *et al* underlined that only the first 29 low-frequency modes (<400 cm^{-1}) contribute to vibrational entropy and found ΔS_{vib} = 44 J.K^{-1}.mol^{-1}. Figure S4 shows vibrational entropy changes obtained in this way from our calculations, based on frequency shifts calculated between HS and LS states.

However, this approach based on equation *(3)* has some limits. First, it requires identifying clearly the corresponding HS and LS λ modes to calculate the $\frac{\nu_\lambda^{LS}}{\nu_\lambda^{HS}}$ ratio for each mode, which is not so easy for all the modes, as the nature of the atomic motions often change between LS and HS states. In addition, some modes are spectroscopically silent, like the A_u modes, or too weak to be detected in one phase or both. This precludes accurate calculation of vibrational entropy based on experimental data only. Finally, equation *(3)* is valid when $h\nu_\lambda \ll kT_{SCO}$, where T_{ST} is the spin transition temperature ($T_{ST} \simeq$ 176 K for [Fe(phen)$_2$(NCS)$_2$]). This approximation is therefore valid for $\nu_\lambda \ll$ 100 cm^{-1}, which excludes Fe-N stretching modes. It is therefore relevant to use DFT calculation for including globally the contribution of all the modes to vibrational entropy.

Hereafter we propose a more global approach to calculate the vibrational entropy of the 609 optical modes, based on the frequencies extracted from our DFT calculations, including intramolecular and intermolecular vibrations with different frequencies and symmetries, as well as lattice libration

modes. We calculated the vibrational entropy difference $\Delta S_{vib} = S_{vib}^{HS} - S_{vib}^{LS}$ by considering the total contribution of the 609 optical modes λ for different spin states:

$$S_{vib}^{SS} = R \sum_{\lambda}^{SS} \left\{ -\ln(1 - e^{-\frac{h\nu_{\lambda}^{SS}}{kT}}) + \frac{h\nu_{\lambda}^{SS}}{kT} \frac{1}{\left(e^{\left(\frac{h\nu_{\lambda}^{SS}}{kT}\right)} - 1 \right)} \right\} \quad (4)$$

where the superscript *SS* stands for HS or LS spin state and $T = T_{ST}$ = 176 K.

Figure 7 shows the contributions to vibrational entropy of the different modes in the crystal in the LS state (blue) and in the HS state (red), in the spectral range below 300 cm^{-1} where vibrational entropy is dominant. The modes above 400 cm^{-1} contribute much less to the total vibrational entropy change, due to low population and weaker frequency shift. The total contributions to vibrational entropy spans from 3.61 $J.K^{-1}.mol^{-1}$ for B_{2g} modes to 4.62 $J.K^{-1}.mol^{-1}$ for B_{1g} modes and the total vibrational entropy change for the 609 optical modes reaches $\Delta S_{vib} = 32.97$ $J.K^{-1}.mol^{-1}$.

Here again we can highlight the important contribution of stretching modes, like the A_g breathing mode shifting from 109 cm^{-1} (HS) to 174 (LS), with $\Delta S_{breathing}^{Ag}$ = 0.87 $J.K^{-1}.mol^{-1}$. The four breathing modes shown in Figure S4 (A_g n°68, A_u n°66, B_{2g} n°65, B_{2u} n°67) of the four molecules in the unit cell have a total contribution $\Delta S_{breathing}$ = 3.2 $J.K^{-1}.mol^{-1}$ similar to the one estimated in previous studies for isolated molecule.[6, 8, 13, 15] However, there are many libration modes (Figure 6) at low frequency contributing to vibrational entropy change, such as the B_{2g} rotational mode shifting from 49 to 53.1 cm^{-1} or the B_{1g} sliding mode shifting from 31.5 (LS) to 24.2 cm^{-1} (HS) with ΔS_{lib} = 0.55 $J.K^{-1}.mol^{-1}$. The contribution to vibrational entropy

change of libration modes below 100 cm^{-1} is 4.2 $J.K^{-1}.mol^{-1}$. We underline again that the simplified approximation of the vibrational entropy, $\Delta S_{vib} = R \sum_{\lambda} \ln(\frac{\nu_{\lambda}^{LS}}{\nu_{\lambda}^{HS}})$ is valid for $\nu_{\lambda} \ll 100$ cm^{-1}. Using this expression for the breathing mode shifting from 174 (LS) to 109 cm^{-1} (HS) overestimate its contribution to 3.84 $J.K^{-1}.mol^{-1}$ compared to 3.44 $J.K^{-1}.mol^{-1}$ obtained from equation *(4)*. The contribution of higher frequency modes, like NCS torsion mode shifting from 313 (LS) to 285 cm^{-1} (HS) is even more overestimated with Eq *(3)* to 0.78 $J.K^{-1}.mol^{-1}$ compared to 0.48 $J.K^{-1}.mol^{-1}$ with Eq *(4)*.

In principle, we should not consider only the frequencies of Brillouin zone center modes, but the ones of all phonon modes within the Brillouin zone, with a dispersion of the phonon frequencies $\nu(k)$ with their wavevector k. Since such calculations cost too much simulation time, it is more reasonable to consider a global softening of the phonon branches from LS to HS states, and therefore a constant $\frac{\nu_{\lambda}^{LS}(k)}{\nu_{\lambda}^{HS}(k)}$ ratio for the different k modes of a λ branch. In addition to optical modes, acoustic modes also contribute to entropy change due to their frequency shift characterized by the speed of sound change. Here again a global softening of the acoustic modes can be considered to change as the speed of sound ratio between LS and HS states, which is of the order of 1.1. Equation (3) is valid for the 3 acoustic branches of the crystal made of unit cells including 4 molecules, and the vibrational entropy change of the acoustic branches reaches: $\Delta S_{ac} = \frac{3}{4} R \, ln(1.1) = 0.6$ $J.K^{-1}.mol^{-1}$.

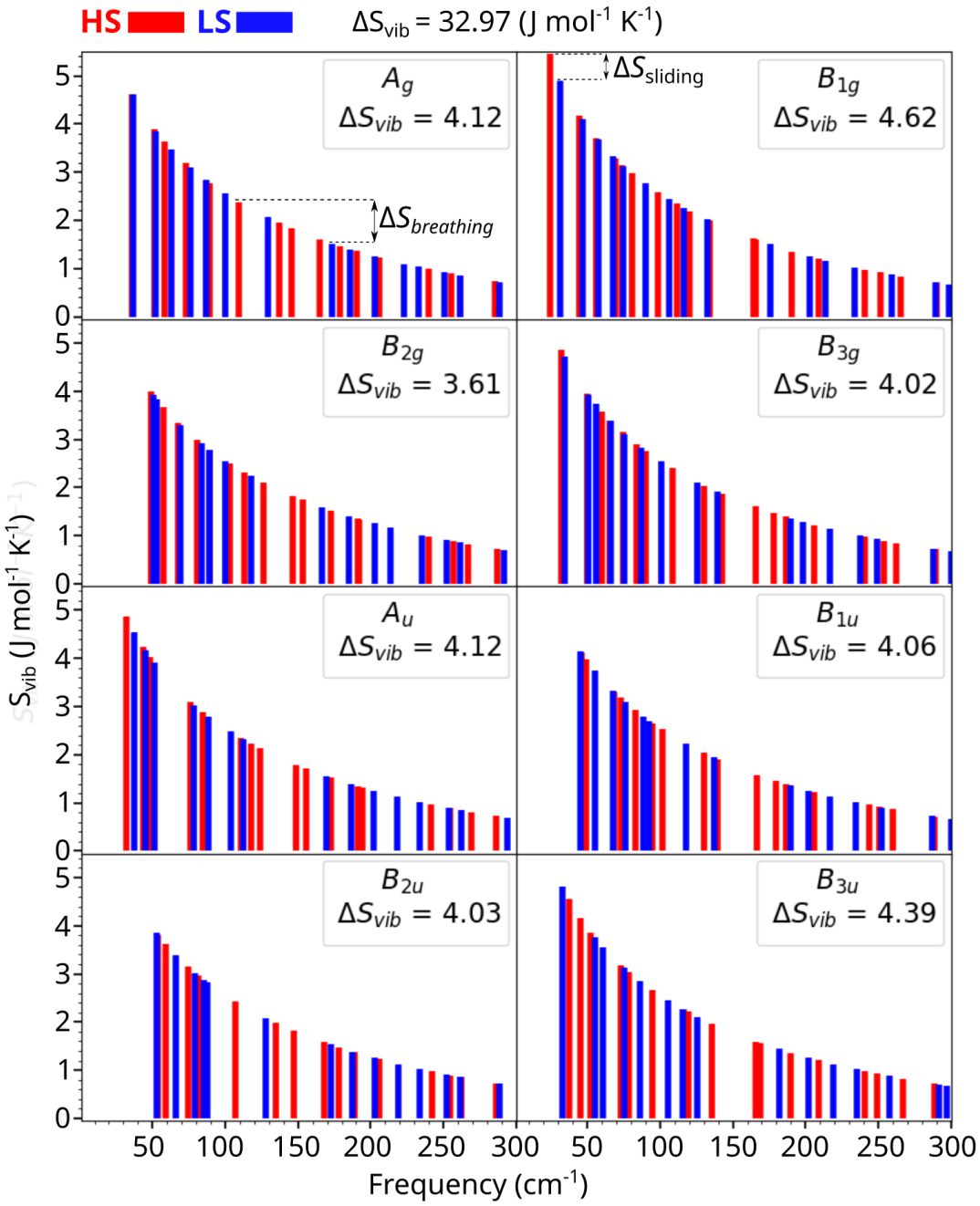

Figure 7. Contribution to vibrational entropy of the optical modes of different symmetries in the spectral range below 300 cm^{-1}. Red bars correspond to HS state and blue bars to LS state. The arrow in the B_{1g} panel corresponds to the variation of vibrational entropy for mode 4 shifting from 31.5 (LS) to 24.2 cm^{-1} (HS). The total vibrational entropy difference ΔS_{vib} given in panels for each symmetries is given in $J.K^{-1}.mol^{-1}$.

Conclusions

This work highlights the complexity of lattice vibrations in molecular crystals made of unit cells including several molecules. Symmetry-resolved spectroscopic measurements allow for selectively probing the frequencies of lattice modes with similar nature but different frequencies, and their frequency splitting is a signature of the libration nature of the modes and of the effect of the inter-molecular packing, as highlighted by DFT calculation. Experimental and theoretical calculations show that most of the modes are strongly affected by the spin transition, and especially the ones below 400 cm^{-1}, which are also the ones with the strongest contribution to vibrational entropy. However, the frequency change of the modes is strongly symmetry dependent. The different respective contributions to entropy change give a total entropy difference $\Delta S = \Delta S_{el} + \Delta S_{vib} + \Delta S_{ac}$ = 46.95 $J.K^{-1}.mol^{-1}$, which is very close to the experimental value of 48.78 $J.K^{-1}.mol^{-1}$.

Our work confirms the important role of vibrational entropy in the entropy-driven spin-crossover phenomena, as underlined by previous pioneering studies, which is enriched by libration modes and inter-molecular modes of different symmetries in crystals.

Supporting Information. The following files are available free of charge.

The supplementary pdf contains the character table of the point group mmm (Table S1) the list of the frequencies of the modes (Table S2), a comparison on powder and single crystal IR data (Figure S1), additional Raman data (Figure S2 and S3) and the contribution of the different modes to vibrational entropy Figure S4. Supplementary videos show the N↔CS modes (video 1), the A_g, A_u, B_{2g} and B_{2u} breathing modes (video 2) and libration modes (video 3).

AUTHOR INFORMATION

Corresponding Author

To whom correspondence should be addressed: eric.collet@univ-rennes1.fr, Jean-Yves.Mevellec@cnrs-imn.fr, alaska.subedi@polytechnique.edu.

Author Contributions

E.C., J.-Y.M., A.S., M.L., E.J., and B.H conceived and coordinated the project in the frame of the ANR ELECTROPHONE projects. G.P., J.-Y.M., G.P., E.C. and B.H. performed the IR and Raman experiment and analyzed the data. N.D. and G.C. synthesized and characterized the samples. A.S. performed the DFT calculations. G.P. and E.C. wrote the manuscript and all authors contributed to discussions and gave comments on the manuscript. All authors have given approval to the final version of the manuscript.

Funding Sources

The authors gratefully acknowledge Agence Nationale de la Recherche for financial support undergrant, ANR-19-CE30-0004 ELECTROPHONE. G.P. thanks Région Bretagne for partial PhD funding (ARED PHONONIC). E.C. thanks the Fondation Rennes1 for funding.

For Table of Contents Use Only

Symmetry-resolved study of lattice vibration and libration modes in $[Fe(phen)_2(NCS)_2]$ crystal

Gaël Privault, Jean-Yves Mevellec, Maciej Lorenc, Bernard Humbert, Etienne Janod Nathalie Daro, Guillaume Chastanet, Alaska Subedi* and Eric Collet**

TOC graphic

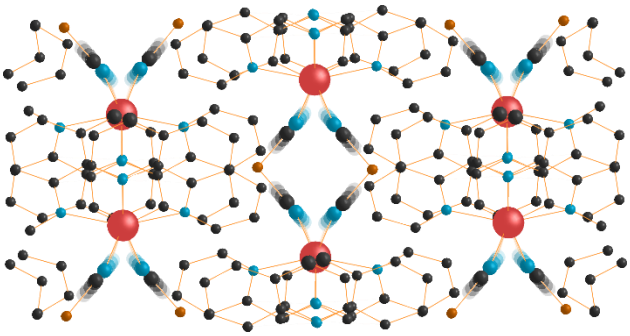

Synopsis: Symmetry-resolved study of lattice vibrations in a spin crossover crystal reveals their complex nature.

References

1. Halcrow, M. A., *Spin-crossover materials : properties and applications*. John Wiley & Sons, Ltd,: Chichester, 2013; p 546.
2. Gutlich, P.; Hauser, A.; Spiering, H., Thermal and Optical Switching of Iron(II) Complexes. *Angewandte Chemie-International Edition in English* **1994,** *33* (20), 2024-2054.
3. Nicolazzi, W.; Bousseksou, A., Thermodynamical aspects of the spin crossover phenomenon. *Cr Chim* **2018,** *21* (12), 1060-1074.
4. Gournay, L.; Chaban, I.; Mevellec, J.-Y.; Humbert, B.; Janod, E.; Guerin, L.; Cammarata, M.; Daro, N.; Chastanet, G.; Collet, E., Shifting photo-stationary light-induced excited spin state trapping equilibrium towards higher temperature by increasing light fluence. *Chemical Physics Letters* **2022,** *791*, 139395.
5. Tissot, A.; Shepherd, H. J.; Toupet, L.; Collet, E.; Sainton, J.; Molnar, G.; Guionneau, P.; Boillot, M. L., Temperature- and Pressure-Induced Switching of the Molecular Spin State of an Orthorhombic Iron(III) Spin-Crossover Salt. *Eur J Inorg Chem* **2013,** (5-6), 1001-1008.
6. Bousseksou, A.; McGarvey, J. J.; Varret, F.; Real, J. A.; Tuchagues, J.-P.; Dennis, A. C.; Boillot, M. L., Raman spectroscopy of the high- and low-spin states of the spin crossover complex $Fe(phen)_2(NCS)_2$: an initial approach to estimation of vibrational contributions to the associated entropy change. *Chemical Physics Letters* **2000,** *318* (4), 409-416.
7. Tuchagues, J. P.; Bousseksou, A.; Molnar, G.; McGarvey, J. J.; Varret, F., The role of molecular vibrations in the spin crossover phenomenon. *Top Curr Chem* **2004,** *235*, 85-103.
8. Molnár, G.; Mikolasek, M.; Ridier, K.; Fahs, A.; Nicolazzi, W.; Bousseksou, A., Molecular Spin Crossover Materials: Review of the Lattice Dynamical Properties. *Ann Phys-Berlin* **2019,** *531* (10), 1900076.
9. Mariette, C.; Trzop, E.; Mevellec, J.-Y.; Boucekkine, A.; Ghoufi, A.; Maurin, G.; Collet, E.; Muñoz, M. C.; Real, J. A.; Toudic, B., Symmetry breakings in a metal organic framework with a confined guest. *Physical Review B* **2020,** *103*, 134103.
10. Azzolina, G.; Bertoni, R.; Ecolivet, C.; Tokoro, H.; Ohkoshi, S.; Collet, E., Landau theory for non-symmetry-breaking electronic instability coupled to symmetry-breaking order parameter applied to Prussian blue analog. *Physical Review B* **2020,** *102* (13), 134104.
11. Trzop, E.; Buron-Le Cointe, M.; Cailleau, H.; Toupet, L.; Molnar, G.; Bousseksou, A.; Gaspar, A. B.; Real, J. A.; Collet, E., Structural investigation of the photoinduced spin conversion in the dinuclear compound {[Fe(bt)(NCS)2]2(bpym)}: toward controlled multi-stepped molecular switches. *Journal of Applied Crystallography* **2007,** *40* (1), 158-164.
12. Moussa, N. O.; Trzop, E.; Mouri, S.; Zein, S.; Molnár, G.; Gaspar, A. B.; Collet, E.; Buron-Le Cointe, M.; Real, J. A.; Borshch, S.; Tanaka, K.; Cailleau, H.; Bousseksou, A., Wavelength selective light-induced magnetic effects in the binuclear spin crossover compound $[Fe(bt)(NCS)_2]_2(bpym)$. *Physical Review B* **2007,** *75* (5), 054101.
13. Ronayne, K. L.; Paulsen, H.; Hofer, A.; Dennis, A. C.; Wolny, J. A.; Chumakov, A. I.; Schunemann, V.; Winkler, H.; Spiering, H.; Bousseksou, A.; Gutlich, P.; Trautwein, A. X.; McGarvey, J. J., Vibrational spectrum of the spin crossover complex [Fe(phen)(2)(NCS)(2)] studied by IR and Raman spectroscopy, nuclear inelastic scattering and DFT calculations. *Physical Chemistry Chemical Physics* **2006,** *8* (40), 4685-4693.
14. Buron-Le Cointe, M.; Hébert, J.; Baldé, C.; Moisan, N.; Toupet, L.; Guionneau, P.; Létard, J. F.; Freysz, E.; Cailleau, H.; Collet, E., Intermolecular control of thermoswitching and

photoswitching phenomena in two spin-crossover polymorphs. *Physical Review B* **2012,** *85*, 064114
15. Brehm, G.; Reiher, M.; Schneider, S., Estimation of the vibrational contribution to the entropy change associated with the low- to high-spin transition in Fe(phen)(2)(NCS)(2) complexes: Results obtained by IR and Raman spectroscopy and DFT calculations. *Journal of Physical Chemistry A* **2002,** *106* (50), 12024-12034.
16. Metatla, A.; Latelli, H.; Nicolazzi, W.; Bousseksou, A., Vibration-driven thermal transition in binuclear spin crossover complexes. *The European Physical Journal B* **2012,** *85* (6), 205.
17. Sorai, M.; Seki, S., Phonon coupled cooperative low-spin 1A1high-spin 5T2 transition in [Fe(phen)2(NCS)2] and [Fe(phen)2(NCSe)2] crystals. *Journal of Physics and Chemistry of Solids* **1974,** *35* (4), 555-570.
18. Takemoto, J. H.; Streusan.B; Hutchins.B, Far-Infrared Spectra of Some Fe(1,10-Phenanthroline)2x2 Complexes. *Spectrochim Acta A* **1974,** *A 30* (3), 827-834.
19. Watanabe, H.; Tanaka, K.; Bréfuel, N.; Cailleau, H.; Létard, J.-F.; Ravy, S.; Fertey, P.; Nishino, M.; Miyashita, S.; Collet, E., Ordering phenomena of high-spin/low-spin states in stepwise spin-crossover materials described by the ANNNI model. *Physical Review B* **2016,** *93*, 014419.
20. Collet, E.; Azzolina, G., Coupling and decoupling of spin crossover and ferroelastic distortion: Unsymmetric hysteresis loop, phase diagram, and sequence of phases. *Physical Review Materials* **2021,** *5* (4), 044401.
21. Azzolina, G.; Bertoni, R.; Collet, E., General Landau theory of non-symmetry-breaking and symmetry-breaking spin transition materials. *Journal of Applied Physics* **2021,** *129* (8), 085106.
22. Lemke, H. T.; Kjær, K. S.; Hartsock, R.; Brandt van Driel, T.; Chollet, M.; Glownia, J. M.; Song, S.; Zhu, D.; Pace, E.; Matar, S. F.; Nielsen, M. N.; Benfatto, M.; Gaffney, K. J.; Collet, E.; Cammarata, M., Coherent structural trapping through wave packet dispersion during photoinduced spin state switching. *Nat. Commun.* **2017,** *8*, 15342.
23. Zerdane, S.; Wilbraham, L.; Cammarata, M.; Iasco, O.; Rivière, E.; Boillot, M. L.; Ciofini, I.; Collet, E., Comparison of structural dynamics and coherence of d–d and MLCT light-induced spin state trapping. *Chem. Sci.* **2017,** *8*, 4978-4986.
24. Chergui, M.; Collet, E., Photoinduced structural dynamics of molecular systems mapped by time-resolved x-ray methods. *Chemical Reviews* **2017,** *117* (16), 11025–11065.
25. Marino, A.; Cammarata, M.; Matar, S. F.; Letard, J. F.; Chastanet, G.; Chollet, M.; Glownia, J. M.; Lemke, H. T.; Collet, E., Activation of coherent lattice phonon following ultrafast molecular spin-state photo-switching: A molecule-to-lattice energy transfer. *Struct Dyn* **2016,** *3* (2), 023605.
26. Bertoni, R.; Cammarata, M.; Lorenc, M.; Matar, S. F.; Létard, J. F.; Lemke, H. T.; Collet, E., Ultrafast light-induced spin-state trapping photophysics investigated in Fe(phen)2(NCS)2 spin-crossover crystal. *Acc Chem Res* **2015,** *48* (3), 774-81.
27. Cammarata, M.; Bertoni, R.; Lorenc, M.; Cailleau, H.; Di Matteo, S.; Mauriac, C.; Matar, S. F.; Lemke, H.; Chollet, M.; Ravy, S.; Laulhe, C.; Létard, J. F.; Collet, E., Sequential Activation of Molecular Breathing and Bending during Spin-Crossover Photoswitching Revealed by Femtosecond Optical and X-Ray Absorption Spectroscopy. *Physical Review Letters* **2014,** *113* (22), 227402.

28. Collet, E.; Azzolina, G.; Ichii, T.; Guerin, L.; Bertoni, R.; Moréac, A.; Cammarata, M.; Daro, N.; Chastanet, G.; Kubicki, J.; Tanaka, K.; Matar, S. F., Lattice phonon modes of the spin crossover crystal [Fe(phen)2(NCS)2] studied by THz, IR, Raman spectroscopies and DFT calculations. *The European Physical Journal B* **2019,** *92* (1), 12.
29. Bertoni, R.; Lorenc, M.; Graber, T.; Henning, R.; Moffat, K.; Létard, J. F.; Collet, E., Cooperative elastic switching vs. laser heating in [Fe(phen)2(NCS)2] spin-crossover crystals excited by a laser pulse. *Crystengcomm* **2016,** *18* (38), 7269-7275.
30. Marchivie, M.; Guionneau, P.; Howard, J. A. K.; Chastanet, G.; Letard, J. F.; Goeta, A. E.; Chasseau, D., Structural characterization of a photoinduced molecular switch. *Journal of the American Chemical Society* **2002,** *124* (2), 194-195.
31. Balde, C.; Desplanches, C.; Wattiaux, A.; Guionneau, P.; Gutlich, P.; Letard, J. F., Effect of metal dilution on the light-induced spin transition in [Fe(x)Zn(1-x)(phen)2(NCS)2] (phen = 1,10-phenanthroline). *Dalton Trans* **2008,** (20), 2702-7.
32. Gallois, B.; Real, J. A.; Hauw, C.; Zarembowitch, J., Structural changes associated with the spin transition in bis(isothiocyanato)bis(1,10-phenanthroline)iron: a single-crystal x-ray investigation. *Inorganic Chemistry* **1990,** *29* (6), 1152-1158.
33. Collet, E.; Azzolina, G.; Ichii, T.; Guerin, L.; Bertoni, R.; Moréac, A.; Cammarata, M.; Daro, N.; Chastanet, G.; Kubicki, J.; Tanaka, K.; Matar, S. F., Lattice phonon modes of the spin crossover crystal [Fe(phen)2(NCS)2] studied by THz, IR, Raman spectroscopies and DFT calculations. *The European Physical Journal B* **2019,** *92* (1).
34. Togo, A.; Tanaka, I., First principles phonon calculations in materials science. *Scripta Materialia* **2015,** *108*, 1-5.
35. Giannozzi, P.; Baroni, S.; Bonini, N.; Calandra, M.; Car, R.; Cavazzoni, C.; Ceresoli, D.; Chiarotti, G. L.; Cococcioni, M.; Dabo, I.; Dal Corso, A.; de Gironcoli, S.; Fabris, S.; Fratesi, G.; Gebauer, R.; Gerstmann, U.; Gougoussis, C.; Kokalj, A.; Lazzeri, M.; Martin-Samos, L.; Marzari, N.; Mauri, F.; Mazzarello, R.; Paolini, S.; Pasquarello, A.; Paulatto, L.; Sbraccia, C.; Scandolo, S.; Sclauzero, G.; Seitsonen, A. P.; Smogunov, A.; Umari, P.; Wentzcovitch, R. M., QUANTUM ESPRESSO: a modular and open-source software project for quantum simulations of materials. *Journal of Physics: Condensed Matter* **2009,** *21* (39), 395502.
36. Garrity, K. F.; Bennett, J. W.; Rabe, K. M.; Vanderbilt, D., Pseudopotentials for high-throughput DFT calculations. *Computational Materials Science* **2014,** *81*, 446-452.
37. Klimeš, J.; Bowler, D. R.; Michaelides, A., Chemical accuracy for the van der Waals density functional. *Journal of Physics: Condensed Matter* **2009,** *22* (2), 022201.
38. Baranovic, G.; Babic, D., Vibrational study of the Fe(phen)(2)(NCS)(2) spin-crossover complex by density-functional calculations. *Spectrochim Acta A* **2004,** *60* (5), 1013-1025.
39. Reiher, M., Theoretical Study of the Fe(phen)2(NCS)2 Spin-Crossover Complex with Reparametrized Density Functionals. *Inorganic Chemistry* **2002,** *41* (25), 6928-6935.
40. Bucko, T.; Hafner, J.; Lebegue, S.; Angyan, J. G., Spin crossover transition of Fe(phen)2(NCS)2: periodic dispersion-corrected density-functional study. *Phys Chem Chem Phys* **2012,** *14* (16), 5389-96.
41. Lindoy, L. F.; Livingstone, S. E., Complexes of iron(II),cobalt(II) and nickel(II) with α-diimines and related bidentate ligands. *Coordination Chemistry Reviews* **1967,** *2* (2), 173-193.
42. Kulshreshtha, S. K.; Iyer, R. M., Nature of the high-spin (5T2) α low-spin (1A1,) transition in [Fe(bipy)2(NCS)2]. *Chemical Physics Letters* **1984,** *108* (5), 501-504.